Progress In Electromagnetics Research C, Vol. 29, 219–234, 2012

DECOUPLED UNITARY ESPRIT ALGORITHM FOR 2-D DOA ESTIMATION

J. Jiang and L. Gan*

School of Electronic Engineering, University of Electronic Science & Technology of China, No. 2006, Xiyuan Ave., West Hi-Tech. Zone, Chengdu, P. R. China

Abstract—In this paper, a new decoupled Unitary ESPRIT algorithm for two-dimensional (2-D) direction-of-arrival (DOA) estimation is presented. By exploiting the centro-symmetric array configurations of two parallel uniform linear arrays (TP-ULAs) and utilizing the via rotational invariance techniques, the proposed algorithm has advantages as listed below. First, the algorithm enables decoupling the estimation problem into a two-step estimation problem and obtains the automatically matched 2-D DOAs. Second, employing the elements of the array fully, the algorithm can estimate 2-D DOAs up to $2(M-1)$, where $2M$ is the sensor number of the array. Besides, the computational complexity of the proposed algorithm is lower than other representative 2-D DOA estimation methods. Simulation results are presented to show the effectiveness of the proposed method.

1. INTRODUCTION

During the past three decades, the problem of two-dimensional (2-D) direction-of-arrival (DOA) estimation based on passive array has attracted much attention, especially in field as radar, sonar, seismology, and radio communication systems. Many 2-D DOA estimation algorithms have been proposed. The most popular methods for distinguishing sources are maximum Likelihood (ML) method [1] and subspace methods [1–3]. The ML method can obtain optimum parameters; however, the computational load of it is so heavy that it is not amenable to real-time implementations. The subspace methods, although not optimal, are computationally more attractive than ML method. But some subspace methods need multidimensional searching

Received 5 April 2012, Accepted 15 May 2012, Scheduled 25 May 2012

* Corresponding author: Lu Gan (ganlu@uestc.edu.cn).

for spectral peaks or the elevation and azimuth angles pair-matching in 2-D DOA estimation. Since these steps cause heavy computational load, the subspace methods can hardly be put to effect. Therefore, it is essential to find an estimator that can overcome the computation burden and have the merits of high resolution and capability to estimate more sources.

Based on the two parallel uniform linear arrays (TP-ULAs), many methods have been presented. Utilizing the geometry of TP-ULAs, Yin et al. [4, 5] proposed a DOA matrix algorithm which has a lower computational load than 2-D MUSIC; however, its performance is poor. It needs to be improved when compared to the CRB [6, 7]. Wu et al. [8] presented a fast estimation method, propagator method(PM), which only uses linear operations to obtain the signal subspace. The method avoids the computational load of eigen-decomposition. Unfortunately, PM for the TP-ULAs fails to work when elevation angles or azimuth angles are between 70° and 90°. Furthermore, additional pair-matching procedure is needed. By exploiting the geometry of TP-ULAs, Xia [9] suggested a 2-D root MUSIC method. This method exploits the array elements fully; therefore, it can achieve high accuracy. Moreover, no pair-matching procedure is needed. TP-ULAs is a special case of uniform rectangle arrays (URA). For the URA, Zoltowski et al. [10] proposed a new 2-D Unitary ESPRIT method, named URA ESPRIT in this paper, which exploits via rotational invariance of URA. The computation of the method is efficient; however, for TP-ULAs, the maximum number of sources that the URA ESPRIT can estimate is only $M-1$, where the sensor number of TP-ULAs is $2M$.

In this paper, a decoupled Unitary ESPRIT method for 2-D DOAs estimation using TP-ULAs is proposed. The proposed method utilizes the centro-symmetric geometry of TP-ULAs and exploits ESPRIT-like structure in terms of real-valued computations throughout. It decouples the 2-D DOA estimation problem into a two-step estimation problem and estimates the elevation and azimuth angles without pair matching procedure. These procedures can reduce computational complexity. Comparison shows that the algorithm has a lower computational load than the URA ESPRIT or Xia's method. Besides, the proposed method has better performance than the DOA matrix algorithm and can estimate 2-D DOAs of up to $2(M-1)$ uncorrelated sources as well as Xia's method.

In the following sections, details of the proposed method are described. In Section 2, the definition and properties of the centro-Hermitian matrix are presented. Then a model of the proposed algorithm is depicted in Section 3.1. Based on TP-ULAs, the decoupled Unitary ESPRIT is derived in Section 3.2. Afterwards,

the procedures of the proposed method are summarized, and its computation complexity is analyzed and compared. In Section 4, simulation results of the algorithm are presented. Finally, some conclusions are drawn in Section 5.

2. CENTRO-HERMITIAN MATRIX

In this section, the centro-Hermitian matrix [11] and its property are reviewed.

Throughout the paper, $\mathbf{\Pi}_p$ denotes the $p \times p$ exchange matrix as

$$\mathbf{\Pi}_p = \begin{bmatrix} 0 & 0 & \dots & 1 \\ 0 & 0 & \dots & 0 \\ \vdots & \vdots & \ddots & \vdots \\ 0 & 1 & \dots & 0 \\ 1 & 0 & \dots & 0 \end{bmatrix} \in \mathbb{R}^{p \times p}. \tag{1}$$

Obviously, $\mathbf{\Pi}_p^2 = \mathbf{I}_p$.

Lee defined the centro-Hermitian matrices [11] as:

Definition 1 *A complex matrix* $\mathbf{M} \in \mathbb{C}^{p \times q}$ *is called centro-Hermitian if*

$$\mathbf{\Pi}_p \mathbf{M}^* \mathbf{\Pi}_q = \mathbf{M} \tag{2}$$

where $(\cdot)^*$ *denotes the complex conjugation of the matrix.*

Lee defines left Π-real matrices [11] as follow to show how centro-Hermitian matrices can be mapped to matrices with real entries

Definition 2 *Matrices* $\mathbf{Q} \in \mathbb{C}^{p \times q}$ *satisfying*

$$\mathbf{\Pi}_p \mathbf{Q}^* = \mathbf{Q} \tag{3}$$

are left Π*-real.*

For example, the left Π-real unitary matrices of even and odd orders are

$$\mathbf{Q}_{2n} = \frac{1}{\sqrt{2}} \begin{bmatrix} \mathbf{I}_n & j\mathbf{I}_n \\ \mathbf{\Pi}_n & -j\mathbf{\Pi}_n \end{bmatrix} \tag{4}$$

$$\mathbf{Q}_{2n+1} = \frac{1}{\sqrt{2}} \begin{bmatrix} \mathbf{I}_n & 0 & j\mathbf{I}_n \\ \mathbf{0}^T & \sqrt{2} & \mathbf{0}^T \\ \mathbf{\Pi}_n & 0 & -j\mathbf{\Pi}_n \end{bmatrix}. \tag{5}$$

Other left Π-real matrices $\mathbf{Q}_s$ can be gained by multiplying the left Π-real $\mathbf{Q}$ by a real matrix $\mathbf{R}$, which means that all the matrices $\mathbf{Q}_s = \mathbf{QR}$ are left -real.

The main results of Lee [11] and Haardt and Nossek [12] are described as:

Theorem 1 *Let* $\mathbf{M} \in \mathbb{C}^{p\times q}$ *be centro-Hermitian, and the matrices* $\mathbf{Q}_p^H\mathbf{M}\mathbf{Q}_q$ *form from* $\mathbf{M}$ *are real, that means* $\mathbf{Q}_p^H\mathbf{M}\mathbf{Q}_q \in \mathbb{R}^{p\times q}$*, where* $\mathbf{Q}_p$ *and* $\mathbf{Q}_q$ *are left* Π*-real matrix define by (4) or (5).*

Theorem 2 *Let* $\mathbf{M} \in \mathbb{C}^{p\times q}$ *be centro-Hermitian, and assume that the SVD of* $\varphi_Q(\mathbf{M}) = \mathbf{Q}_p^H\mathbf{M}\mathbf{Q}_q \in \mathbb{R}^{p\times q}$ *is given by* $\varphi_Q(\mathbf{M}) = \mathbf{U}\mathbf{\Sigma}\mathbf{V}^H \in \mathbb{R}^{p\times q}$*, the SVD of* M *is obtained as*

$$\mathbf{M} = (\mathbf{Q}_p\mathbf{U})\mathbf{\Sigma}(\mathbf{Q}_q\mathbf{V})^H \tag{6}$$

where $\mathbf{Q}_p$ *and* $\mathbf{Q}_q$ *are left* Π*-real matrix defined by (4) or (5). The left and right singular vectors of* M *can be easily proofed to be left* Π*-real.*

3. DECOUPLED UNITARY ESPRIT ALGORITHM

3.1. Data Model

Consider that the model of TP-ULAs is depicted in Figure 1 and that the sensors are located on the x-y plane. The subarray along the x-axis is denoted as ULA1, while the ULA paralleling ULA1 is denoted as ULA2. Each of the ULA contains M sensors with spacing d_1, and the displacement between ULA1 and ULA2 is d_2. Suppose that N far-field narrowband uncorrelated plane sources $s_n(t)\,(n = 1, 2, \ldots, N)$ impinge on the array from different DOA $(\alpha_n, \beta_n)\,(n = 1, 2, \ldots, N, 0 < \alpha_n < \pi, 0 < \beta_n < \pi)$, where α_n and β_n denote the elevation and azimuth angles between the sources and x-axis together with y-axis positive direction,

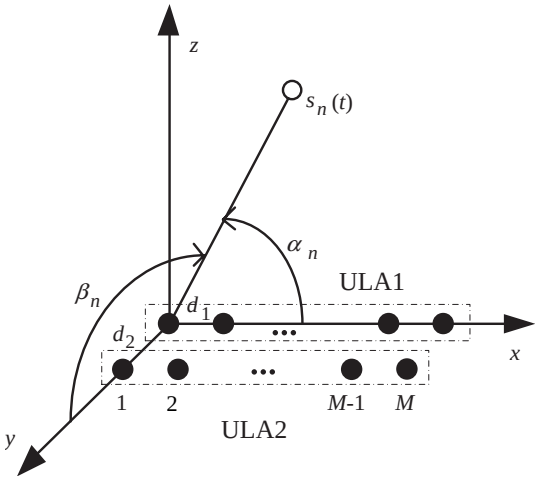

Figure 1. Two parallel uniform linear arrays.

respectively. The observed signals of the tth snapshot measured by ULA1 and ULA2 are

$$\begin{cases} \mathbf{x}_1(t) = \mathbf{A}(\alpha)\mathbf{s}(t) + \mathbf{n}_1(t) \\ \mathbf{x}_2(t) = \mathbf{A}(\alpha)\mathbf{A}(\beta)\mathbf{s}(t) + \mathbf{n}_2(t) \end{cases} \tag{7}$$

where,

$$\begin{aligned} \mathbf{x}_1(t) &= [x_{11}(t), x_{12}(t), \ldots, x_{1M}(t)]^T \\ \mathbf{x}_2(t) &= [x_{21}(t), x_{22}(t), \ldots, x_{2M}(t)]^T \\ \mathbf{A}(\alpha) &= [\mathbf{a}(\mu_1), \mathbf{a}(\mu_2), \ldots, \mathbf{a}(\mu_N)] \\ \mathbf{a}(\mu_n) &= [1, e^{j\mu_n}, \ldots, e^{j(M-1)\mu_n}]^T \\ \mu_n &= 2\pi d_1 \cos\alpha_n/\lambda \\ \mathbf{A}(\beta) &= \mathrm{diag}[a(\beta_1), a(\beta_2), \ldots a(\beta_N)] \\ a(\beta_n) &= \exp(j2\pi d_2 \cos\beta_n/\lambda) \\ \mathbf{s}(t) &= [s_1(t), s_2(t), \ldots, s_N(t)]^T \\ \mathbf{n}_1(t) &= [n_{11}(t), n_{12}(t), \ldots, n_{1M}(t)]^T \\ \mathbf{n}_2(t) &= [n_{21}(t), n_{22}(t), \ldots, n_{2M}(t)]^T. \end{aligned} \tag{8}$$

$(\cdot)^T$ denotes the transpose. $x_{im}(t)$ represents the mth array data in subarray i ($m = 1, 2, \ldots, M$, $i = 1, 2$). $\mathbf{A}(\alpha)$ and $\mathbf{A}(\alpha)\mathbf{A}(\beta)$, which contain the 2-D DOA information of sources and denote the array response vectors of ULA1 and ULA2, respectively. $\mathbf{n}_1(t)$ and $\mathbf{n}_2(t)$ are the temporal and spatial additive white gaussian noise (AWGN) vectors, with zero mean and variance σ^2.

For simplicity, $\mathbf{s}(t)$, $\mathbf{x}_i(t)$ and $\mathbf{n}_i(t)$ are marked as $\mathbf{s}$, $\mathbf{x}_i$ and $\mathbf{n}_i$, where $i = 1, 2$. The output $\mathbf{X}$ measured by the array is

$$\mathbf{X} = \begin{pmatrix} \mathbf{x}_1 \\ \mathbf{x}_2 \end{pmatrix} = \begin{pmatrix} \mathbf{A}(\alpha) \\ \mathbf{A}(\alpha)\mathbf{A}(\beta) \end{pmatrix} \mathbf{s} + \begin{pmatrix} \mathbf{n}_1 \\ \mathbf{n}_2 \end{pmatrix} = \mathbf{B}\mathbf{s} + \mathbf{n} \tag{9}$$

where $\mathbf{B} \triangleq \begin{pmatrix} \mathbf{A}(\alpha) \\ \mathbf{A}(\alpha)\mathbf{A}(\beta) \end{pmatrix}$.

For utilizing the rotational invariance techniques, the partition method of the array is considered as depicted in Figure 2. To choose the subarray1 and subarray2, the chosn matrix $\mathbf{J}$ is defined as

$$\mathbf{J} = \begin{bmatrix} \mathbf{J}_1 \\ \mathbf{J}_2 \end{bmatrix} \tag{10}$$

where $\mathbf{J}_1 = \begin{bmatrix} 1 & 0 \\ 0 & 1 \end{bmatrix} \otimes \mathbf{J}_1'$, $\mathbf{J}_2 = \begin{bmatrix} 1 & 0 \\ 0 & 1 \end{bmatrix} \otimes \mathbf{J}_2'$, $\mathbf{J}_1' = \begin{bmatrix} \mathbf{I}_{M-1} & 0_{(M-1)\times 1} \end{bmatrix}$, $\mathbf{J}_2' = \begin{bmatrix} 0_{(M-1)\times 1} & \mathbf{I}_{M-1} \end{bmatrix}$. $\bigotimes$ presents the Kronecker product.

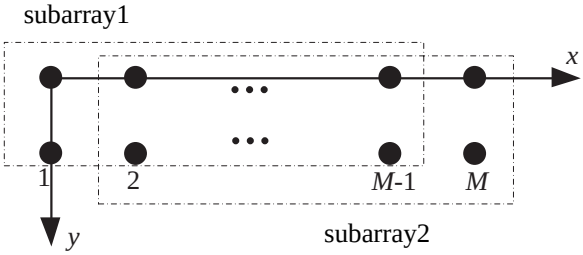

Figure 2. The subarray partition of the array.

Then the new steering matrix can be obtained by multiplying the steering matrix $\mathbf{B}$ with the chosen matrix $\mathbf{J}$ on the left. It can be obtained

$$\begin{cases} \mathbf{A}_1 = \mathbf{J}_1\mathbf{B} \\ \mathbf{A}_2 = \mathbf{J}_2\mathbf{B} \end{cases} \tag{11}$$

where $\mathbf{A}_1$ and $\mathbf{A}_2$ present the steering matrices of the subarray1 and subarray2. Therefore,

$$\mathbf{A}_1 = \begin{bmatrix} \mathbf{A}_{1:M-1}(\alpha) \\ \mathbf{A}_{1:M-1}(\alpha)\mathbf{A}(\beta) \end{bmatrix} \tag{12}$$

$$\mathbf{A}_2 = \begin{bmatrix} \mathbf{A}_{2:M}(\alpha) \\ \mathbf{A}_{2:M}(\alpha)\mathbf{A}(\beta) \end{bmatrix} = \begin{bmatrix} \mathbf{A}_{1:M-1}(\alpha) \\ \mathbf{A}_{1:M-1}(\alpha)\mathbf{A}(\beta) \end{bmatrix} \mathbf{\Phi} = \mathbf{A}_1\mathbf{\Phi} \tag{13}$$

where $\mathbf{A}_{1:M-1}(\alpha)$ denotes the steering matrix of the first $M-1$ array along the x axis, while $\mathbf{A}_{2:M}(\alpha)$ denotes the steering matrix of the last $M-1$ array along the x axis. $\mathbf{\Phi} = \text{diag}\left\{e^{j\mu_n}\right\}_{n=1}^{N}$, where $\mu_n = 2\pi d_1 \cos\alpha_n/\lambda$, and μ_n only contains the information of elevation angles. The symbol $\text{diag}(\cdot)$ represents the diagonal matrix.

Consider that the output data $\mathbf{X}$ is noiseless for simple derivation. Premultiplying $\mathbf{X}$ by $\mathbf{J}$ yields the following equation:

$$\mathbf{JX} = \begin{bmatrix} \mathbf{X}_1 \\ \mathbf{X}_2 \end{bmatrix} = \begin{bmatrix} \mathbf{A}_1 \\ \mathbf{A}_2 \end{bmatrix} \mathbf{s} = \begin{bmatrix} \mathbf{A}_1 \\ \mathbf{A}_1\mathbf{\Phi} \end{bmatrix} \mathbf{s} \tag{14}$$

where $\mathbf{X}_1$ and $\mathbf{X}_2$ are the outputs measured by the subarray1 and the subarray2.

3.2. Decoupled Unitary ESPRIT Algorithm

According to (8) and (10), the steering matrix of the TP-ULAs satisfies

$$\mathbf{\Pi}_{2M}\mathbf{B}^* = \mathbf{B}\mathbf{\Lambda} \tag{15}$$

where $\mathbf{\Lambda} = \mathrm{diag}\left\{\left(e^{j(M-1)p_i}a(\beta_i)\right)_{i=1}^{N}\right\}$ is a diagonal matrix.

With the hypothesis that no additive noise exists, the Unitary ESPRIT data matrix is defined as

$$\mathbf{Z} = [\mathbf{X}\ \mathbf{\Pi}_{2M}\mathbf{X}^*]. \tag{16}$$

Multiply (16) by $\mathbf{J}$ from the left, we can obtain

$$\mathbf{JZ} = \begin{bmatrix}\mathbf{X}_1 & \mathbf{\Pi}_M\mathbf{X}_2{}^* \\ \mathbf{X}_2 & \mathbf{\Pi}_M\mathbf{X}_1{}^*\end{bmatrix} = \begin{bmatrix}\mathbf{A}_1 \\ \mathbf{A}_1\mathbf{\Phi}\end{bmatrix}\left[\mathbf{s}\ \mathbf{\Phi}^{-1}\mathbf{\Lambda}\mathbf{s}^*\right] = \mathbf{B}_J\left[\mathbf{s}\ \mathbf{\Phi}^{-1}\mathbf{\Lambda}\mathbf{s}^*\right] \tag{17}$$

where $\mathbf{B}_J = (\mathbf{A}_1^T, (\mathbf{A}_1\mathbf{\Phi})^T)^T$. Obviously, $rank(\mathbf{Z}) = rank(\mathbf{X}) = N$, thus $\mathbf{Z}$ is rank-deficient. Equations (13), (16) and (17) imply that the equivalent measurements of array double from L to $2L$, where L is the snapshot number. Therefore, compared to the standard ESPRIT, the estimation accuracy of the proposed algorithm will increase.

Then, define a matrix

$$\mathbf{Z}' = [\mathbf{X}\ \mathbf{\Pi}_{2M}\mathbf{X}^*\mathbf{\Pi}_L] = [\mathbf{X}\ \mathbf{\Pi}_{2M}\mathbf{X}^*]\begin{bmatrix}\mathbf{I}_L & \\ & \mathbf{\Pi}_L\end{bmatrix} = \mathbf{ZG}. \tag{18}$$

Clearly, $\mathbf{G} = \begin{bmatrix}\mathbf{I}_L & \\ & \mathbf{\Pi}_L\end{bmatrix}$, $\mathbf{GG}^T = \mathbf{I}_{2L}$, thus $\mathbf{G}^{-1} = \mathbf{G}^T = \mathbf{G}^H$.

Furthermore,

$$\mathbf{\Pi}_{2M}\left(\mathbf{Z}'\right)^*\mathbf{\Pi}_{2L} = \mathbf{\Pi}_{2M}(\mathbf{ZG})^*\mathbf{\Pi}_{2L} = \mathbf{Z}'. \tag{19}$$

Hence, $\mathbf{Z}'$ is a centro-Hermitian matrix.

According to *Theorem* 1, the matrix

$$\mathbf{P} = \mathbf{Q}_{2M}^H\mathbf{Z}'\mathbf{Q}_{2L} \tag{20}$$

is real matrix.

And it can be written as

$$\mathbf{P} = \mathbf{Q}_{2M}^H\left[\mathbf{X}\ \mathbf{\Pi}_{2M}\mathbf{X}^*\mathbf{\Pi}_L\right]\mathbf{Q}_{2L} = \left[\Re\left\{\mathbf{Y}\right\}, \Im\left\{\mathbf{Y}\right\}\right] \tag{21}$$

where $\mathbf{Y} = \mathbf{Q}_{2M}^H\mathbf{X}$.

The autocorrelation matrix of $\mathbf{P}$ is

$$\begin{aligned}\mathbf{R}_{\mathbf{P}} &= E\left[\mathbf{P}\mathbf{P}^H\right] \\ &= E\left[\left(\mathbf{Q}_{2M}^H\mathbf{Z}'\mathbf{Q}_{2L}\right)\left(\mathbf{Q}_{2M}^H\mathbf{Z}'\mathbf{Q}_{2L}\right)^H\right] \\ &= E\left[\mathbf{Q}_{2M}^H\mathbf{ZGQ}_{2L}\mathbf{Q}_{2L}^H(\mathbf{ZG})^H\mathbf{Q}_{2M}\right]\end{aligned} \tag{22}$$

where $E[\cdot]$ denotes the expectation. With $\mathbf{Q}_{2L}\mathbf{Q}_{2L}^H = \mathbf{I}$, $\mathbf{GG}^H = \mathbf{I}$ and (18), (22) can be simplified as

$$\mathbf{R}_{\mathrm{P}} = \mathbf{Q}_{2M}^H\mathbf{R}_Z\mathbf{Q}_{2M} \tag{23}$$

where $\mathbf{R}_Z = E\left[\mathbf{Z}\mathbf{Z}^H\right]$.

The singular value decomposition (SVD) of $\mathbf{P}$ is

$$\mathbf{P} = \mathbf{U}\boldsymbol{\Sigma}\mathbf{V}^H \tag{24}$$

where $\mathbf{U}$ is the matrix whose columns are the left singular vectors of $\mathbf{P}$, $\mathbf{V}$ the matrix whose columns are the right singular vectors of $\mathbf{P}$, and $\boldsymbol{\Sigma}$ the diagonal matrix constructed by the singular values of $\mathbf{P}$.

Rewrite the autocorrelation matrix of $\mathbf{R_P}$,

$$\mathbf{R_P} = E\left[\mathbf{P}\mathbf{P}^H\right] = \begin{bmatrix} \mathbf{U}_s & \mathbf{U}_n \end{bmatrix} \begin{bmatrix} \boldsymbol{\Sigma}_s & \\ & \boldsymbol{\Sigma}_n \end{bmatrix} \begin{bmatrix} \mathbf{U}_s \\ \mathbf{U}_n \end{bmatrix}^H \tag{25}$$

where $\mathbf{U}_s$ is the signal subspace spanned by the left singular vectors corresponding to the N largest singular values of $\mathbf{P}$, while $\mathbf{U}_n$ is the noise subspace spanned by the rest singular vectors. $\boldsymbol{\Sigma}_s$ and $\boldsymbol{\Sigma}_n$ are the diagonal matrix of the N largest singular values and the rest smallest singular values. Because it has been considered that no additive noise exists, the noise subspace and its transform must be null. To keep consistent with most subspace methods, the noise subspace presentation is reserved in the following derivation.

Combining (23) with (25), it yields

$$\mathbf{Q}_{2M}^H \mathbf{R}_Z \mathbf{Q}_{2M} = \begin{bmatrix} \mathbf{U}_s & \mathbf{U}_n \end{bmatrix} \begin{bmatrix} \boldsymbol{\Sigma}_s & \\ & \boldsymbol{\Sigma}_n \end{bmatrix} \begin{bmatrix} \mathbf{U}_s \\ \mathbf{U}_n \end{bmatrix}^H. \tag{26}$$

Therefore,

$$\mathbf{R}_Z = \mathbf{Q}_{2M}\mathbf{U}_s\boldsymbol{\Sigma}_s(\mathbf{Q}_{2M}\mathbf{U}_s)^H + \mathbf{Q}_{2M}\mathbf{U}_n\boldsymbol{\Sigma}_n(\mathbf{Q}_{2M}\mathbf{U}_n)^H \quad . \tag{27}$$

With (17), it is gained

$$\mathbf{R}_{JZ} = E\left[(\mathbf{J}\mathbf{Z})(\mathbf{J}\mathbf{Z})^H\right] = \mathbf{J}E\left[\mathbf{Z}\mathbf{Z}^H\right]\mathbf{J}^H = \mathbf{J}\mathbf{R}_Z\mathbf{J}^H. \tag{28}$$

Combining (28) with (27), it is obtained

$$\mathbf{R}_{JZ} = \mathbf{J}\mathbf{Q}_{2M}\mathbf{U}_s\boldsymbol{\Sigma}_s(\mathbf{J}\mathbf{Q}_{2M}\mathbf{U}_s)^H + \mathbf{J}\mathbf{Q}_{2M}\mathbf{U}_n\boldsymbol{\Sigma}_n(\mathbf{J}\mathbf{Q}_{2M}\mathbf{U}_n)^H. \tag{29}$$

Clearly, $\mathbf{J}\mathbf{Q}_{2M}\mathbf{U}_s\boldsymbol{\Sigma}_s(\mathbf{J}\mathbf{Q}_{2M}\mathbf{U}_s)^H$ is the signal subspace, while $\mathbf{J}\mathbf{Q}_{2M}\mathbf{U}_n\boldsymbol{\Sigma}_n(\mathbf{J}\mathbf{Q}_{2M}\mathbf{U}_n)^H$ is the noise subspace.

With the definition of (17), (28) can be written as

$$\begin{aligned} \mathbf{R}_{JZ} &= E\left[(\mathbf{J}\mathbf{Z})(\mathbf{J}\mathbf{Z})^H\right] \\ &= \mathbf{B}_J E\left[\mathbf{s}\mathbf{s}^H + \boldsymbol{\Phi}^{-1}\boldsymbol{\Lambda}\mathbf{s}\mathbf{s}^H\boldsymbol{\Lambda}^H\left(\boldsymbol{\Phi}^{-1}\right)^H\right]\mathbf{B}_J{}^H. \end{aligned} \tag{30}$$

Obviously, $E\left[\mathbf{s}\mathbf{s}^H + \boldsymbol{\Phi}\boldsymbol{\Lambda}\mathbf{s}\mathbf{s}^H\boldsymbol{\Lambda}^H\left(\boldsymbol{\Phi}^{-1}\right)^H\right]$ is a diagonal matrix.

Thus, the signal subspace $\mathbf{J}\mathbf{Q}_{2M}\mathbf{U}_s\mathbf{\Sigma}_s(\mathbf{J}\mathbf{Q}_{2M}\mathbf{U}_s)^H$ must satisfy,

$$\mathbf{J}\mathbf{Q}_{2M}\mathbf{U}_s = \mathbf{B}_J\mathbf{T} = \mathbf{J}\mathbf{B}\mathbf{T} \tag{31}$$

where $\mathbf{T}$ is a $N \times N$ dimensional non-singular matrix.

Accordingly,

$$\mathbf{Q}_{2M}\mathbf{U}_s = \mathbf{B}\mathbf{T}. \tag{32}$$

Equation (32) denotes the relationship between the signal subspace $\mathbf{U}_s$ of data matrix $\mathbf{Z}$ and the steering matrix $\mathbf{B}$.

Substituting (11) into (32), we can obtain

$$\begin{bmatrix} \mathbf{J}_1 \\ \mathbf{J}_2 \end{bmatrix} \mathbf{Q}_{2M}\mathbf{U}_s = \begin{bmatrix} \mathbf{J}_1 \\ \mathbf{J}_2 \end{bmatrix} \mathbf{B}\mathbf{T} = \begin{bmatrix} \mathbf{A}_1 \\ \mathbf{A}_1\mathbf{\Phi} \end{bmatrix} \mathbf{T}. \tag{33}$$

Thus,

$$\begin{cases} \mathbf{J}_1\mathbf{Q}_{2M}\mathbf{U}_s = \mathbf{A}_1\mathbf{T} \\ \mathbf{J}_2\mathbf{Q}_{2M}\mathbf{U}_s = \mathbf{A}_1\mathbf{\Phi}\mathbf{T} = (\mathbf{A}_1\mathbf{T})\,\mathbf{T}^{-1}\mathbf{\Phi}\mathbf{T}. \end{cases} \tag{34}$$

And it can be rewritten as

$$\mathbf{J}_2\mathbf{Q}_{2M}\mathbf{U}_s\mathbf{T}^{-1} = (\mathbf{J}_1\mathbf{Q}_{2M}\mathbf{U}_s)\,\mathbf{T}^{-1}\mathbf{\Phi}. \tag{35}$$

Multiplying both sides of (35) by $\mathbf{Q}^H_{2(M-1)}$ on the left, it is obtained

$$\mathbf{Q}^H_{2(M-1)}\mathbf{J}_2\mathbf{Q}_{2M}\mathbf{U}_s\mathbf{T}^{-1} = \mathbf{Q}^H_{2(M-1)}\mathbf{J}_1\mathbf{Q}_{2M}\mathbf{U}_s\mathbf{T}^{-1}\mathbf{\Phi}. \tag{36}$$

With Equations $\mathbf{\Pi}_{2(M-1)}\mathbf{J}_2\mathbf{\Pi}_{2M} = \mathbf{J}_1$, $\mathbf{J}_2^* = \mathbf{J}_2$, $\mathbf{\Pi}_{2(M-1)}\mathbf{Q}_{2(M-1)} = \mathbf{Q}^*_{2(M-1)}$ and $\mathbf{\Pi}_{2(M-1)}\mathbf{\Pi}_{2(M-1)} = \mathbf{I}_{2(M-1)}$, $\mathbf{Q}^H_{2(M-1)}\mathbf{J}_1\mathbf{Q}_{2M}$ can be rewritten as [10]

$$\mathbf{Q}^H_{2(M-1)}\mathbf{J}_1\mathbf{Q}_{2M} = (\mathbf{Q}^H_{2(M-1)}\mathbf{J}_2\mathbf{Q}_{2M})^*. \tag{37}$$

Then, the elevation angles α can be estimated using the method for ULA in [10]

$$\mathbf{K}_2\mathbf{U}_s = \mathbf{K}_1\mathbf{U}_s\mathbf{T}^{-1}\mathbf{\Omega}\mathbf{T} \tag{38}$$

where $\mathbf{\Omega} = \mathrm{diag}\left\{\tan\left(\mu_n/22\right)\right\}_{n=1}^{N}$, $\mu_n = 2\pi d_1 \cos\alpha_n/\lambda$, $\mathbf{K}_1 \triangleq \Re\left\{\mathbf{Q}^H_{2(M-1)}\mathbf{J}_2\mathbf{Q}_{2M}\right\}$, $\mathbf{K}_2 \triangleq \Im\left\{\mathbf{Q}^H_{2(M-1)}\mathbf{J}_2\mathbf{Q}_{2M}\right\}$.

Thus, it is implied that

$$(\mathbf{K}_1\mathbf{U}_s)^\dagger\mathbf{K}_2\mathbf{U}_s = \mathbf{T}^{-1}\mathbf{\Omega}\mathbf{T} \tag{39}$$

where, the superscript $(^\dagger)$ denotes Moore-Penrose inverse.

Then, using the singular value decomposition, $(\mathbf{K}_1\mathbf{U}_s)^\dagger\mathbf{K}_2\mathbf{U}_s$ can be written as

$$(\mathbf{K}_1\mathbf{U}_s)^\dagger\mathbf{K}_2\mathbf{U}_s = \mathbf{U}_K\mathbf{\Lambda}_K\mathbf{U}_K^{-1} \tag{40}$$

where, $\mathbf{\Lambda}_K = \mathrm{diag}\,(\gamma_1, \gamma_2, \ldots, \gamma_N)$ is the diagonal matrix constructed by the eigenvalues $\gamma_1, \gamma_2, \ldots, \gamma_N$ of $(\mathbf{K}_1\mathbf{U}_s)^\dagger\mathbf{K}_2\mathbf{U}_s$, and $\mathbf{U}_K$ is the matrix constructed by the eigenvectors corresponding to the eigenvalues $\gamma_1, \gamma_2, \ldots, \gamma_N$. Therefore, the eigenvalues of $(\mathbf{K}_1\mathbf{U}_s)^\dagger\mathbf{K}_2\mathbf{U}_s$ are equal to diagonal elements of $\mathbf{\Omega}$, and the columns of $\mathbf{T}^{-1}$ are eigenvectors of $(\mathbf{K}_1\mathbf{U}_s)^\dagger\mathbf{K}_2\mathbf{U}_s$.

$$\mathbf{T}^{-1} = \mathbf{U}_K \tag{41}$$

$$\mu_n = 2\tan^{-1}(\gamma_n)\,,\; n = 1, 2, \ldots, N\,. \tag{42}$$

Accordingly, the elevation angles α can be obtained by solving the following equation

$$\alpha_n = \cos^{-1}\left[\frac{\lambda\mu_n}{2\pi d_1}\right], \quad n = 1, 2, \ldots, N. \tag{43}$$

With (32) and the estimated matrix $\mathbf{T}^{-1}$, we can obtain

$$\hat{\mathbf{B}} = \mathbf{Q}_{2M}\mathbf{U}_s\mathbf{T}^{-1}. \tag{44}$$

The matrix $\hat{\mathbf{B}}$ can be divided into two submatrices with the same dimension defined by $\hat{\mathbf{B}} = \left[\hat{\mathbf{B}}_1^T, \hat{\mathbf{B}}_2^T\right]^T$.

With the definition of (9), $\hat{\mathbf{B}}$ can be rewritten as

$$\hat{\mathbf{B}} = \begin{bmatrix} \hat{\mathbf{B}}_1 \\ \hat{\mathbf{B}}_2 \end{bmatrix} = \begin{bmatrix} \mathbf{A}\,(\alpha) \\ \mathbf{A}\,(\alpha)\,\mathbf{A}\,(\beta) \end{bmatrix}. \tag{45}$$

Rearrange Equation (45) as:

$$\mathbf{A}\,(\beta) = (\mathbf{A}\,(\alpha))^\dagger\mathbf{A}\,(\alpha)\,\mathbf{A}\,(\beta) = \left(\hat{\mathbf{B}}_1\right)^\dagger\hat{\mathbf{B}}_2. \tag{46}$$

Thus, the azimuth angles can be estimated,

$$\beta_n = \cos^{-1}\left(\frac{\lambda\arg\left(a(\beta_n)\right)}{2\pi d_2}\right)\;\; n = 1, \ldots, N\,. \tag{47}$$

where, $a(\beta_n)$ is the nth diagonal element of matrix $\mathbf{A}\,(\beta)$.

Because of the one-to-one correspondence between the eigenvalues and the eigenvectors of $(\mathbf{K}_1\mathbf{U}_s)^\dagger\mathbf{K}_2\mathbf{U}_s$, estimated elevation angles and azimuth angles will match each other automatically.

3.3. Summary of the Proposed Method

Procedures of the proposed estimation method are summarized as follows.

(i) Calculate the sample autocorrelation matrix $\mathbf{R}_{\mathrm{P}}$ according to (21)

$$\begin{aligned}\hat{\mathbf{R}}_{\mathrm{P}} &= \frac{1}{2N_s}\left(\mathrm{P}\mathrm{P}^T\right) \\ &= \frac{1}{2L}\left(\left(\Re\left\{\mathbf{Y}\right\}\right)\left(\Re\left\{\mathbf{Y}\right\}\right)^T + \Im\left\{\mathbf{Y}\right\}\left(\Im\left\{\mathbf{Y}\right\}\right)^T\right)\end{aligned}$$

where, $\mathbf{Y} = \mathbf{Q}_{2M}^H\mathbf{X}$, L is the number of snapshots.

(ii) Extract the N eigen-vectors associated with the biggest singular values of $\mathbf{R_P}$ to form the $2M \times N$ dimensional signal subspace $\mathbf{U}_s$.

(iii) Compute the diagonal matrix $\hat{\mathbf{\Omega}}$ and eigenvector matrix $\hat{\mathbf{T}}$ by eigenvalue decomposition of the unitary matrix $(\mathbf{K}_1\mathbf{U}_s)^\dagger\mathbf{K}_2\mathbf{U}_s$.

(iv) Estimate the steering matrix $\mathbf{B}$ according to the equation $\mathbf{B} = \mathbf{Q}_{2M}\mathbf{U}_s\mathbf{T}^{-1}$.

(v) Estimate elevation angles and azimuth angles by (43) and (47).

The computational loads of the proposed method with DOA matrix algorithm, URA ESPRIT and Xia's method are compared. Generally, the number L of snapshots is much greater than the number of sensors $2M$. The number of flops required for the complex product is more than four times of the real product required, where a flop is defined as a real floating-point addition or multiplication operations. Calculating the sample covariance matrix requires the order of M^2L [13]. The eigenvalue decomposition or singular value decomposition of a $M \times M$ matrix is about $O\left(M^3\right)$ [13]. The flops of the rooting steps are assumed to be not higher than $O\left(M^3\right)$ [13]. Table 1 shows the computational complexity of different methods for 2-D estimation. The proposed method is more efficient than DOA matrix algorithm, URA ESPRIT and Xia's method.

4. COMPUTER SIMULATION RESULTS

Computer simulations are carried out to illustrate the performance of the proposed algorithm. The simulation results of the DOA matrix

Table 1. Computational complexity.

Operation	Real	Complex
DOA matrix algorithm	–	$2M^2L + O\left(M^3\right)$
URA ESPRIT	$O\left((2M)^3\right)$	$O\left(((2M)-1)^3\right)$
Xia's method	–	$(2M)^2L + O\left((2M)^3\right)$
The proposed method	$2\,(2M)^2L + O\left((2M)^3\right)$	–

algorithm, URA ESPRIT method, and Xia's method are included in contrast to the performance of the proposed algorithm. The sensors of the array are assumed to be lying along x-y plane as shown in Figure 1. The number of sensors in each ULA is $M = 5$, with sensor displacement $d_1 = d_2 = \lambda/2$. λ is the wavelength of incident signals.

Example 1: The simulation results of these algorithms are presented in the presence of noise firstly. Assume that a narrow-band signal impinges upon the array from the 2-D angles $(\alpha, \beta) = (50°, 60°)$. The number of snapshots is $L = 512$. The SNR varies from -10 dB to 20 dB. The performance of the estimators can be obtained from 10000 times individual computer simulations, by calculating the root mean square errors (RMSE) of the estimated 2-D DOAs. The RMSEs are defined as

$$RMSE\,(\alpha) = \sqrt{E\left[(\hat{\alpha} - \alpha)^2\right]}$$

$$RMSE\,(\beta) = \sqrt{E\left[\left(\hat{\beta} - \beta\right)^2\right]}.$$

And the total RMSE is defined as

$$RMSE\,(\alpha, \beta) = \sqrt{E[(\hat{\alpha} - \alpha)^2 + (\hat{\beta} - \beta)^2]}.$$

Figure 3, Figure 4, and Figure 5 show RMSEs for the elevation angle α, azimuth angle β, and the total RMSE of azimuth and elevation angles, respectively, versus different SNR conditions. Clearly, the performance of the proposed method is similar to the URA ESPRIT and Xia's method, and better than the DOA matrix algorithm. The RMSE of elevation angle α of the proposed method and URA ESPRIT

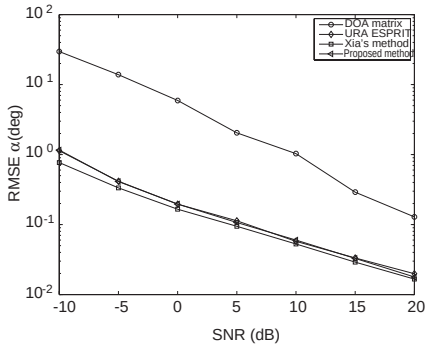

Figure 3. The RMSE (α) for the signal versus SNR.

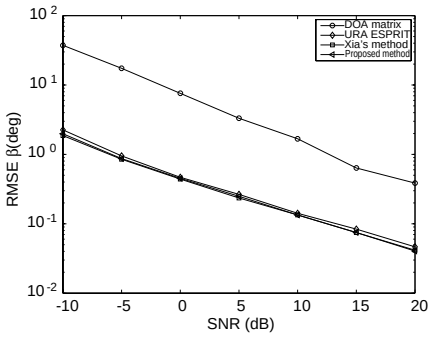

Figure 4. The RMSE (β) for the signal versus SNR.

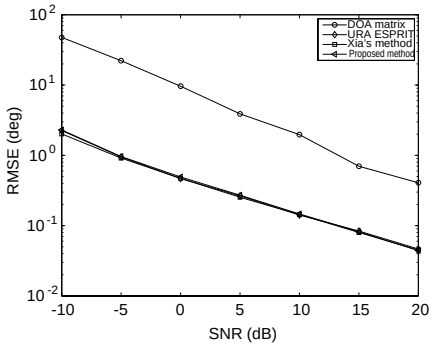

Figure 5. The total RMSE for the signal versus SNR.

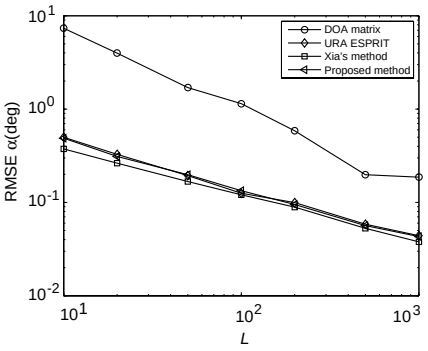

Figure 6. The RMSE (α) for the signal versus snapshot number.

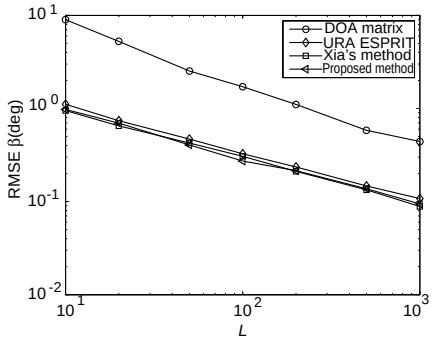

Figure 7. The RMSE (β) for the signal versus snapshot number.

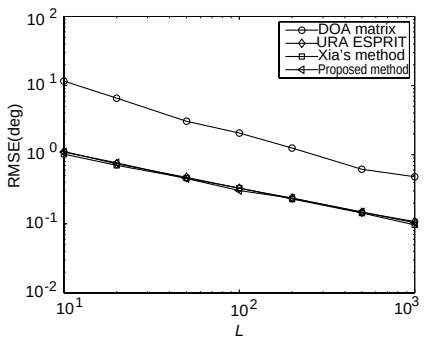

Figure 8. The total RMSE for the signal versus snapshot number.

are a little weaker than Xia's method, because Xia's method is a root-finding-based method. And the RMSEs of azimuth angle β of the proposed method and Xia's method are better than URA ESPRIT. The proposed method can achieve the same performance as Xia's method and is applicable with computational advantages compared to other algorithms.

Example 2: This experiment is included to compare the performance of the proposed method with DOA matrix algorithm, URA ESPRIT and Xia's method against different snapshots. SNR $= 10$ dB, and the other conditions are the same as in *Example* 1.

Figure 6, Figure 7, and Figure 8 show the RMSEs of elevation

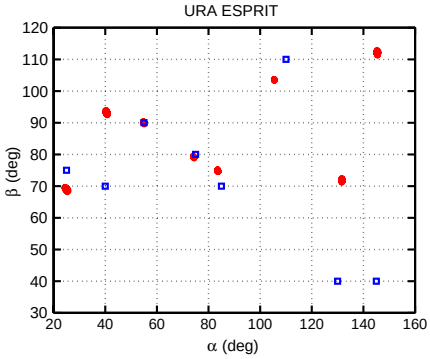

Figure 9. The hash map of URA ESPRIT (The blue symbol '□' denotes theoretical values of the angles, while the red symbol '◯' denotes the estimated values).

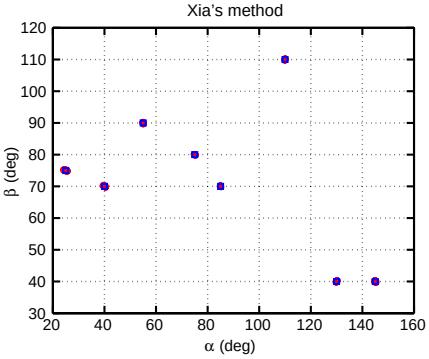

Figure 10. The hash map of Xia's method (The blue symbol '□' denotes theoretical values of the angles, while the red symbol '◯' denotes the estimated values).

angle α, azimuth angle β, and the total RMSE of azimuth and elevation angle, respectively, versus different snapshots number conditions. As shown in Figure 7, Figure 6, and Figure 8, the proposed method can obtain a similar performance to URA ESPRIT and Xia's method in the present of different snapshots, while the DOA matrix algorithm achieves poor performance. It is noted that the proposed method has a considerable resolution with very few snapshots.

Example 3: The maximum number of sources that these algorithms can estimate is checked out in the following simulation.

In the example, the number of snapshots at each sensor is assumed 512 and SNR = 10 dB. The uncorrelated narrowband signals are generated with (25°, 75°), (40°, 70°), (55°, 90°), (75°, 80°), (85°, 70°), (110°, 110°), (130°, 40°), and (145°, 40°), which are the same as in Xia's paper. The performance of the estimators is obtained from 100 Monte-Carlo simulations. The hash maps of estimated angles show as follows.

Figure 9 shows that the URA ESPRIT method fails to estimate DOAs when the sources number is $2(M-1)$. But Xia's method and the proposed method can handle up to $2(M-1)$ source signals, as shown in Figure 10 and Figure 11. When the azimuth angles share the same angle 40°, the two methods still work well. It is ascribed that the proposed method and Xia's method employ the array elements efficiently.

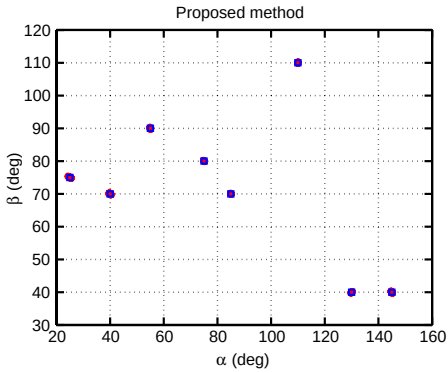

Figure 11. The hash map of the proposed method.

5. CONCLUSIONS

A new Unitary ESPRIT algorithm for 2-D DOA estimation is proposed. The procedure in terms of real-valued computations throughout the algorithm can reduce the computational load efficiently, especially the cost of the complex SVD. The proposed method can handle 2-D DOAs up to $2(M-1)$ uncorrelated sources even if some of them share a common azimuth angle or elevation angle. Besides, the pair-matching procedure of the angles is automatic, which can also reduce the computational load. The proposed method brings about so many computational superiorities relative to the existing 2-D estimation approaches, without a reduction of estimation accuracy. Computer simulations are carried out to demonstrate the performance of the proposed method.

ACKNOWLEDGMENT

This work was supported by 'the Fundamental Research Funds for the Central Universities' (Grant No. ZYGX2010J027) and CAEP fund (Grant No. 2010A0403017).

REFERENCES

1. Chan, A. Y. J. and J. Litva, "MUSIC and maximum likelihood techniques on two-dimensional DOA estimation with uniform circular array," *IEE Proceedings — Radar, Sonar and Navigation*, Vol. 142, No. 3, 105–114, 1995.

2. Kedia, V. S. and B. Chandna, "A new algorithm for 2-D DOA estimation," *Signal Processing*, Vol. 60, No. 3, 325–332, 1997.
3. Van der Veen, A. J., P. B. Ober, and E. F. Deprettere, "Azimuth and elevation computation in high resolution DOA estimation," *IEEE Transactions on Signal Processing*, Vol. 40, No. 7, 1828–1832, 1992.
4. Yin, Q. Y., R. W. Newcomb, and L. H. Zou, "Estimating 2-D angles of arrival via two parallel linear arrays," *1989 International Conference on Acoustics, Speech, and Signal Processing, ICASSP-89*, Vol. 4, 2803–2806, 1989.
5. Yin, Q.-Y., et al., "Relation between the DOA matrix method and the ESPRIT method," *IEEE International Symposium on Circuits and Systems*, Vol. 2, 1561–1564, 1990.
6. Nehorai, A. and E. Paldi, "Vector-sensor array processing for electromagnetic source localization," *IEEE Transactions on Signal Processing*, Vol. 42, No. 2, 376–398, 1994.
7. See, C. M. S. and A. B. Gershman, "Direction-of-arrival estimation in partly calibrated subarray-based sensor arrays," *IEEE Transactions on Signal Processing*, Vol. 52, No. 2, 329–338, 2004.
8. Wu, Y., G. Liao, and H. C. So, "A fast algorithm for 2-D direction-of-arrival estimation," *Signal processing*, Vol. 83, No. 8, 1827–1831, 2003.
9. Xia, T., et al., "Decoupled estimation of 2-D angles of arrival using two parallel uniform linear arrays," *IEEE Transactions on Antennas and Propagation*, Vol. 55, No. 9, 2627–2632, 2007.
10. Zoltowski, M. D., M. Haardt, and C. P. Mathews, "Closed-form 2-D angle estimation with rectangular arrays in element space or beamspace via unitary ESPRIT," *IEEE Transactions on Signal Processing*, Vol. 44, No. 2, 316–328, 1996.
11. Lee, A., "Centrohermitian and skew-centrohermitian matrices," *Linear Algebra and Its Applications*, Vol. 29, 205–210, 1980.
12. Haardt, M. and J. A. Nossek, "Unitary ESPRIT: How to obtain increased estimation accuracy with a reduced computational burden," *IEEE Transactions on Signal Processing*, Vol. 43, No. 5, 1232–1242, 1995.
13. Golub, G. H. and C. F. Van Loan, *Matrix Computations,* Johns Hopkins University Press, 1996.